G Protein-Coupled Glutamate and GABA Receptors Form Complexes and Mutually Modulate Their Signals

Hakushun Sakairi[1], Yuji Kamikubo[1], Masayoshi Abe[2], Keisuke Ikeda[2], Arata Ichiki[2], Toshihide Tabata[2], Masanobu Kano[3], Takashi Sakurai[1]

Author affiliations:

[1]Department of Pharmacology, Juntendo University School of Medicine, Hongo 2-1-1, Bunkyo-ku, Tokyo 113-8421, Japan

[2]Laboratory for Biological Information Processing, Faculty of Engineering and Graduate School of Science and Engineering, University of Toyama, 3190 Gofuku, Toyama, Toyama 930-8555, Japan

[3]Department of Neurophysiology, Graduate School of Medicine, The University of Tokyo, 7-3-1 Hongo, Tokyo 113-0033, Japan

All correspondence should be addressed to:

Yuji Kamikubo, PhD

Department of Pharmacology, Juntendo University School of Medicine

Hongo 2-1-1, Bunkyo-ku, Tokyo 113-8421, Japan

E-mail: ykamiku@juntendo.ac.jp

Fax: +81-(0)3-5802-0419

Phone: +81-(0)3-5802-1035

ABSTRACT

Molecular networks containing various proteins mediate many types of cellular processes. Elucidation of how the proteins interact will improve our understanding of the molecular integration and physiological and pharmacological propensities of the network. One of the most complicated and unexplained interactions between proteins is the inter-G-protein coupled receptor (GPCR) interaction. Recently, many studies have suggested that an interaction between neurotransmitter GPCRs may mediate diverse modalities of neural responses. The B-type gamma-aminobutyric acid (GABA) receptor (GBR) and type-1 metabotropic glutamate receptor (mGluR1) are GPCRs for GABA and glutamate, respectively, and each plays distinct roles in controlling neurotransmission. We have previously reported the possibility of their functional interaction in central neurons. Here, we examined the interaction of these GPCRs using stable cell lines and rat cerebella. Cell-surface imaging and coimmunoprecipitation analysis revealed that these GPCRs interact on the cell surface. Furthermore, fluorometry revealed that these GPCRs mutually modulate signal transduction. These findings provide solid evidence that mGluR1 and GBR have intrinsic abilities to form complexes and to mutually modulate signaling. These findings indicate that synaptic plasticity relies on a network of proteins far more complex than previously assumed.

KEYWORDS:

GPCR, complex formation, metabotropic glutamate receptor, B-type gamma-amino butyric acid receptor, live cell imaging, signaling crosstalk

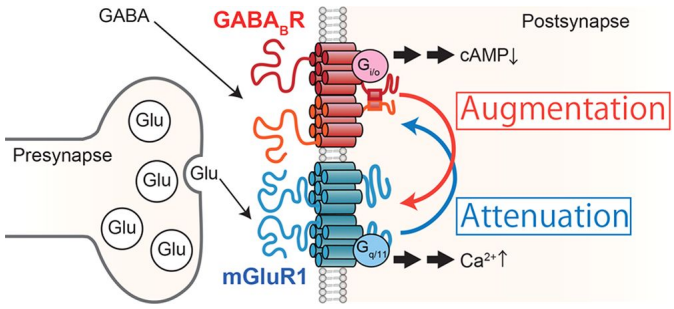
GABA
GABA$_B$R
Postsynapse
$G_{i/o}$
cAMP↓
Augmentation
Glu
Presynapse
Glu
Glu
Glu
Glu
Attenuation
$G_{q/11}$
Ca^{2+}↑
mGluR1

Introduction

Proteins rarely act alone; the molecular machines constructed from multiple interacting proteins play crucial roles in cells. These protein networks mediate many types of cellular processes, including signal transduction, intracellular trafficking, gene expression, and cell metabolism.[1] Recently, many studies have suggested the interaction between membrane proteins including G protein-coupled receptors (GPCRs). GPCRs belong to a large protein superfamily comprising more than 1% of the total human genome. GPCRs respond to various ligands and mediate diverse modalities of cellular responses.[2-4] A single functional GPCR is usually a homo- or heteromeric dimer of the subunits. For example, the type-1 metabotropic glutamate receptor (mGluR1), a G_q/G_{11} protein-coupled receptor for the excitatory neurotransmitter glutamate, is a homodimer of the mGluR1 subunits. By contrast, the gamma-aminobutyric acid (GABA) B receptor (GBR), a G_i/G_o protein-coupled receptor for the inhibitory neurotransmitter GABA,[5-7] is a heterodimer of the GBR1 and GBR2 subunits.[8] In the past two decades, many studies have further expanded the notion of inter-GPCR interaction; a functional GPCR forms a complex with other functional GPCRs, and such a GPCR complex can mediate cellular responses that each GPCR alone cannot mediate.[9]

In the cerebellar cortex, individual Purkinje cells integrate excitatory synaptic inputs from numerous parallel fibers (i.e., the axons of granule cells), relaying mossy fiber inputs that convey sensory information arising from various parts of the body and motor command signals from the upper centers.[10] The efficacy of transmission at certain parallel fiber–Purkinje cell synapses undergoes long-term depression (cerebellar LTD) following temporally correlated transmission at these synapses and climbing fiber–Purkinje cell synapses.[11] Cerebellar LTD is recognized as a cellular basis for cerebellum-dependent motor learning and memory.[11] Activation of mGluR1 in Purkinje cells is a key step inducing cerebellar LTD.

It remains a mystery that a high density of GBR is localized on the annuli of parallel fiber-innervated Purkinje cell dendritic spines.[12, 13] GBR appears to be useless at these glutamatergic

synapses. A hypothesis can be derived from the fact that GBR expression highly overlaps with mGluR1 expression at the annuli: [14, 15] GBR could modulate some cellular responses by interacting with mGluR1. As GBR and mGluR1 are colocalized at the perisynaptic region of dendritic spines, transmitter molecules that diffuse away from the synaptic cleft (spillover) can activate these extrasynaptic receptors.[16, 17] Furthermore, GABA and glutamate are contained in the cerebrospinal fluid, and their concentrations are regulated in various situations.[18] Tonic and phasic GABA may activate postsynaptic GBR to control mGluR1 signaling. In this work, we investigated whether and how GBR may interact with mGluR1 and the cellular responses mediated through this inter-GPCR interaction. As many types of GPCRs and the related signal molecules are natively expressed in Purkinje cells, it is difficult to precisely investigate the details of the structural and functional interaction between mGluR1 and GBR in Purkinje cells. Therefore, we attempted to reconstruct the interaction of these GPCRs in a heterologous expression system using cell lines. Use of the reconstruction system allowed us to focus on and observe target GPCR interactions at the molecular level and to dissect the underlying molecular mechanisms. We created stably transfected HEK293 cells with a tetracycline (Tet)-inducible expression of these GPCRs. Coimmunoprecipitation (Co-IP) and cell surface imaging analysis revealed that GBR and mGluR1colocalize and form complexes on the cell surface. Consistent with previous studies in native Purkinje cells,[14, 19, 20] Ca^{2+} imaging showed that activation of GBR enhances mGluR1 signaling in HEK293 cells. Furthermore, a cAMP bioassay showed that mGluR1 activation inhibits GBR signaling. These findings together show that mGluR1 and GBR form complexes and modulate each other.

Result and Discussion

GBR1, GBR2, and mGluR1 Form Complexes

Since membrane protein complexes are affected by cellular conditions and extraction buffer, the complex formation of mGluR1 and GBR in the central nervous system or heterogeneous cell lines is controversial.[15, 19, 21] To examine the possibility of complex formation of mGluR1 and GBRs in the central nervous system, we first performed co-IP experiments from the lysates of the crude synaptosomal fraction derived from female rat cerebella. In the immunoblot of the fractions precipitated with the anti-mGluR1 antibody, immunoreactivity for GBR1 was found at the corresponding molecular weights (~120 kDa; Figure1 A). Consistent with this result, mGluR1 and GBR2 were detected at the corresponding molecular weights (~150 kDa and ~120 kDa, Figure 1 B) in the precipitates with anti-GBR1 antibody.

We assessed the possibility of complex formation of mGluR1 and GBR in a transient expression system. We performed co-IP studies using HEK293 cells transfected with GBR1 fused with the HA tag at the C-terminus (GBR1-HA), GBR2 fused with the VSVG tag at the C-terminus (GBR2-VSVG), and mGluR1 fused with the Venus tag at the C-terminus (mGluR1-Venus). In the fraction precipitated with a Venus-reactive anti-GFP antibody, immunoreactivities for GBR1-HA and GBR2-VSVG were detected at the corresponding molecular weights (~120 kDa, Figure 1 C).

For detailed evaluation of the physiological response to the complex formed by mGluR1 and GBR, we established stable HEK293 cell lines showing Tet-dependent expression of mGluR1 and GBR1 (HEKmg1, Figure 1 D clone #01), mGluR1 and GBR2 (HEKmg2, Figure 1 D clone #03), or mGluR1, GBR1, and GBR2 (HEKmg12, Figure 1 D clones #04 and #12). After treatment with 2 μM doxycycline (Dox) for > 6 h, expression of these receptors was detectable in the clones (Figure S1). In co-IP experiments with fractions of HEKmg12 cells precipitated with the anti-mGluR1 antibody, GBR1 and GBR2 were detected at the corresponding molecular weights (Figure 1 E). As a corollary, mGluR1 was detected in immunoprecipitates obtained with the anti-GBR1 or anti-GBR2 antibodies (Figure 1 F). Furthermore, our co-IP analysis with HEKmg1 and HEKmg2 showed that

either GBR1 or GBR2 alone can form complexes with mGluR1 (Figure 1 G). These results indicated that there is complex formation and colocalization in HEK cells and neurons (Figure 1). Since mGluR1 and GBR interact with many membrane proteins, they may mediate the formation of these GPCR complexes. [21, 22] Based on these results, we attempted to reconstruct the interaction between mGluR1 and GBR using HEK293 cells with a Tet-inducible expression system as a cellular model.

Cell Surface Colocalization and Interaction of GBR and mGluR1

We examined whether GBR-mGluR1 colocalization would occur on the cell surface using cell-surface labeling and total internal reflection fluorescence (TIRF) microscopy to selectively excite fluorophores near the adherent cell surface.[23] We performed live-cell multicolor TIRF imaging using HEK293 cells transiently transfected with GBR1 fused with the SNAP tag at the N-terminus (SNAP-GBR1), GBR2 fused with the VSVG tag at the N-terminus (VSVG-GBR2), and mGluR1 fused with the HA tag at the N-terminus (HA-mGluR1). For post-translational-surface labeling, cells were treated with SNAP-surface 488 (cell-impermeable SNAP tag substrate), DyLight (DL) 649 labeled anti-VSVG, and AF 594 labeled anti-HA antibodies at room temperature for 30 min (Table S1). A TIRF imaging of the surface-labeled GPCRs revealed substantial levels of colocalization, suggesting interaction at the plasma membrane (Figure 2 A). These results showed the possibility of colocalization and complex formation of these GPCRs on the cell surface of HEK293 cells.

We performed TIRF imaging of fixed HEKmg12 cells stained with the anti-N terminus of the GBR1, GBR2, and mGluR1 antibodies as primary antibodies and subsequently stained with fluorescently labeled secondary antibodies (Figure 2 B, C; Table S1). As shown in the line scans of the fluorescent intensities detected on the merge images (shown as dotted arrows), the fluctuation of AF488 and AF594 fluorescent intensities is corresponding. The experiments indicated that there was colocalization of these GPCRs on the cell surface or within ~200 nm above the plane of the cell-glass contact surface.

Moreover, we performed antibody patching analysis of cell-surface GPCRs on HEKmg12 cells by TIRF microscopy. In the antibody patching assay, incubation with an antibody directed to the extracellular domain of the membrane protein, followed by a fluorescently labeled secondary antibody, induced protein patches. Coaccumulation of the proteins in or around the patches indicated interactions with the patch-forming proteins. The antiextracellular domain of the GBR1 antibody followed by an AF 488-labeled secondary antibody (Table S1) induced patches on the surface of living HEK293 mg12 cells. After washing and fixation, HEKmg12 cells were stained with anti-GBR2, anti-mGluR1, or anti-NAKA antibodies (Figure 2 D F) directed to the intracellular domain, followed by an AF594-labeled secondary antibody (Table S1). We analyzed the correlation coefficient of colocalization. The correlation between GBR1 and mGluR1 was higher than that between GBR1 and NAKA (Figure 2 G, $p = 0.0087$, Wilcoxon rank sum test with Bonferroni correction), suggesting that part of GBR1 may physically interact with mGluR1 on the cell membrane. The above results suggested colocalization and complex formation of GBR1, GBR2, and mGluR1 on the cell surface of HEKmg12 cells. These receptors endogenously colocalize at the perisynaptic region of dendritic spines.[12, 24] Our results together indicate that we successfully established a cell line that reconstructed the assembly of these GPCRs previously suggested in native neurons. In addition, only some GPCRs may come in sufficiently tight contact to interact with each other in the heterologous expression system because obvious mutual functional modulation between the GPCRs was not observed in some cells (see the next section).

GBR Activation Augmented mGluR1 Signaling

We previously showed that GBR activation leads to an increase in the ligand-sensitivity of mGluR1 in cerebellar Purkinje cells.[14, 19] Here, we investigated whether GBR-mediated mGluR1 sensitization occurs in the non-neuronal cellular environment of HEKmg12 cells and dissected the mechanisms underlying this phenomenon, taking advantage of the manipulatable heterologous gene expression. In HEK293 cells, heterologously expressed mGluR1 can couple to the G_q/G_{11} protein–

protein kinase C cascade.[25] The G_q/G_{11} protein may also mediate signaling to intracellular Ca^{2+} mobilization in this cell type.[26] Fluorometry showed that a 2-s local application of 50 μM (*RS*)-3,5-dihydroxyphenylglycine (DHPG, a group-I mGluR agonist) evoked a transient increase in the intracellular Ca^{2+} concentration in HEKmg12 cells (Figure 3A). A 12-s conditioning with the control vehicle did not change the peak amplitude of DHPG-evoked Ca^{2+} responses in most cases (Figure 3 A). By contrast, a 12-s conditioning with 30 nM (RS)-4-amino-3-(4-chlorophenyl)butanoic acid (baclofen, a GBR-selective agonist) often augmented the peak amplitude (Figure 3 A). For the control vehicle, the augmentation extent of the peak amplitude rarely exceeded 60% (exceeded in only 4.55% of 22 examined cells, Figure 3 B, C), and the maximal extent was 98.0% (Figure 3 C). For baclofen, 26.5% of the 34 examined cells displayed augmentation extents of ≥ 60% (Figure 3 B, C), and the maximal extent achieved was 651.6% (Figure 3 B). There was a significant difference in the fractional population of the cells with augmentation extents of ≥ 60% between these two conditions ($p = 0.024$, chi-square likelihood ratio test; Figure 3 C). This result suggested that GBR activation may modulate mGluR1 signaling in the non-neuronal cellular environment. Moreover, the conditioning itself did not change the intracellular Ca^{2+} concentration regardless of control vehicle or baclofen (Figure 3 D), suggesting that baclofen may exert mGluR1 signaling augmentation without affecting the intracellular Ca^{2+} mobilization machinery.

We then examined the possibility that the augmentation of the DHPG-evoked Ca^{2+} response is due to an increase in the ligand-sensitivity of mGluR1. In the HEK293 cells used, an application of ≤ 5 μM DHPG alone did not evoke a Ca^{2+} response (Figure 3 E), suggesting that this concentration is below the activation threshold of the mGluR1-coupled response in HEK293 cells. An additional application of control vehicle also did not evoke a Ca^{2+} response in any of the 46 examined cells (Figure 3 E, F). By contrast, an additional application of 30 nM baclofen evoked a Ca^{2+} response in 8.1% of the 37 examined cells (Figure 3 E, F). There was a significant difference in the fractional population of the cells showing Ca^{2+} responses between these two conditions ($p = 0.026$, chi-square likelihood ratio test; Figure 3 F). This result supports the aforementioned possibility.

We assessed whether and how mGluR1 sensitization mediated by GBR may occur in response to the endogenous GBR agonist GABA. A previous electrophysiological study[27] using cerebellar slice preparations reported that GABA may be spilt over from the synaptic terminals of interneurons in the cerebellar cortex; a resultant response increase in the extracellular GABA concentration may exert a short-term modulatory effect on Purkinje cells. To mimic such a short-term action observed *in situ*, we restricted the duration of the GABA application to 2 s by codelivering GABA with DHPG (50 μM, 2 s). We measured the augmentation extent of the peak amplitude of the 50 μM DHPG-evoked Ca^{2+} response by coapplying various concentrations of GABA to HEKmg12 cells (Figure 3 G). Remarkable augmentations were observed at a GABA concentration of 300 nM–1 μM (Figure 3 H). The maximal extent of augmentation achieved similar levels at a GABA concentration of 300 nM–1 μM. The EC_{50} estimated from the Hill function fitted to the data (Figure 3 H, sigmoid curve) was ~60 nM.

GBR Augments mGluR1 Signaling Independently of G_i/G_o Protein

We assessed the involvement of G_i/G_o protein coupled to GBR in the mediation of mGluR1 signaling augmentation through two different approaches. One was to examine the resistance of the augmentation to pertussis toxin (PTX), a G_i/G_o protein inhibitor, while the other was to examine whether the augmentation could be mimicked by mastoparan, a G_i/G_o protein activator. For the first approach, we measured the augmentation extent of the peak amplitude of the 50 μM DHPG-evoked Ca^{2+} response after a 12-s conditioning with 30 nM baclofen in the cells pretreated with 500 ng/mL PTX for 24 h (Figure 4 A). The fractional population of the PTX-pretreated cells with augmentation extents of ≥ 60% was 24.1% (N =87 cells; Figure 4 B, C). This fractional population was not significantly different from that of the nontreated cells (26.5%, data reproduced from Figure 3; p = 0.79, chi-square likelihood ratio test). The baclofen conditioning itself did not considerably change the intracellular Ca^{2+} concentration in the PTX-pretreated cells (Figure. 4 D). To confirm the potency of the PTX pretreatment, we used a luminescent assay to compare the cAMP concentrations of the

lysates of PTX-pretreated and nonpretreated cells after a 15 min incubation with forskolin (FK), an adenylyl cyclase activator (30 nM), and baclofen (30 μM). The cAMP concentration was significantly higher in the lysate of the PTX-treated cells than in the non-pretreated cells ($p = 0.0003$, unpaired t-test; Figure 4 E). This result suggested that the PTX pretreatment indeed inhibited the GBR-coupled G_i/G_o protein, which hampered cAMP production by adenylyl cyclase.

For the second approach, we measured the augmentation extent of the peak amplitude of the DHPG-evoked Ca^{2+} response after a 100-s conditioning with 1 μM mastoparan in nonpretreated cells expressing GBR and mGluR1 (Figure 4 A). None of the 25 examined cells displayed extents of ≥ 60% (Figure 4 B, C). The fractional population of the non-pretreated cells showing augmentation extents of ≥ 60% after mastoparan conditioning (0.0%) was significantly smaller than that after baclofen conditioning (26.5%, data reproduced from Figure 3 C; $p = 0.0009$, chi-square likelihood ratio test). The conditioning itself did not change the intracellular Ca^{2+} concentration, regardless of the treatment (Figure 4 D). To confirm the potency of mastoparan, we used the luminescent assay to compare the cAMP concentrations of the lysates of non-pretreated cells after a 100-s incubation with 30 nM FK and either control vehicle or 1 μM mastoparan. cAMP concentrations were significantly lower in the lysate of the mastoparan-conditioned cells than in the lysate of the control vehicle-conditioned cells ($p = 0.022$, unpaired t-test; Figure 4 F). This result suggested that the mastoparan conditioning indeed activated the GBR-coupled G_i/G_o protein, which hampered cAMP production by adenylyl cyclase.

Functional GBR Is Required to Initiate mGluR1 Signaling Augmentation

A functional GBR consists of the GBR1 subunit responsible for ligand binding and the GBR2 subunit responsible for G_i/G_o protein coupling.[28] Our co-IP analysis showed that either GBR1 or GBR2 alone can form complexes with mGluR1, although they differ in their affinity to mGluR1 (Figure 1 G). To examine whether either of these subunits alone can initiate mGluR1 signaling augmentation, we measured the augmentation extent of the peak amplitude of the 50 μM

DHPG-evoked Ca^{2+} response after a 12-s conditioning with 30 nM baclofen in the cells expressing mGluR1 and either GBR1 or GBR2 (Figure 4 G). The fractional populations of the cells with extents of ≥ 60% were 5.8% for the GBR1-expressing cells (N = 52 cells) and 0.0% for the GBR2-expressing cells (N = 20 cells; Figure 4 H, I). These fractional populations were significantly smaller than those of the cells expressing mGluR1, GBR1, and GBR2 (26.5%, data reproduced from Figure 3 C; $p = 0.007$ and 0.0022, chi-square likelihood ratio test, respectively). This result suggested that functional GBR containing both GBR1 and GBR2 would be required to initiate mGluR1 signaling augmentation. The conditioning did not change the intracellular Ca^{2+} concentration regardless of the expressed subunits (Figure 4 J), suggesting that neither the GBR subunits nor functional GBR affect the intracellular Ca^{2+} mobilization machinery.

mGluR1 Activation Attenuated GBR Signaling

We examined whether and how mGluR1 may modulate GBR signaling, based on the ability of GBR to inhibit cAMP production when stimulated,[29] as GBR is a G_i/G_o protein-coupled receptor. We measured the intracellular cAMP concentrations using the LANCE cAMP assay, a homogeneous time-resolved fluorescence resonance energy transfer (TR-FRET) immunoassay designed to measure intracellular cAMP. Here, we measured the fluorescent intensity at emission of 665 nm (Em665) and 615 nm (Em615) with excitation at 340 nm, and the ratio of Em665 to Em615 (TR-FRET signal) was used to quantify the cAMP.[30] In this assay, TR-FRET signals showed a negative correlation to the cAMP concentrations and were decreased by 30 nM FK (Figure S2). To enable the measurement of the GBR-mediated reduction in the intracellular cAMP, the basal cAMP was raised by treatment with FK and phosphodiesterase inhibitor, 3-isobutyl 1-methylxanthine (IBMX). Using this assay system, we validated that GBR activation suppressed the FK-mediated TR-FRET signal reduction in HEKmg12 cells. When the cells were treated with baclofen in the presence of FK, the FK-induced suppression of the TR-FRET signal was inhibited (Figure 5 A open circle). Next, to evaluate the effect of mGluR1 activation on GBR signaling, we treated HEKmg12 cells with baclofen in the

presence of FK and DHPG. The baclofen-mediated inhibition of cAMP production was reduced by 10 μM DHPG application (Figure 5 A closed square, $p < 0.01$, two-way analysis of variance [ANOVA]). Our further analyses indicated that GBR-mediated cAMP reduction was suppressed by DHPG at a dose of 10–300 μM (Figure 5 B, $p < 0.01$, one-way ANOVA). Additionally, we independently confirmed mGluR1-mediated GBR signaling attenuation using bioluminescent cAMP assays to measure intracellular cAMP concentrations (Figure S3).

We confirmed whether baclofen would affect the intracellular cAMP pathway without GBR using an HEK293 cell line expressing mGluR1 without GBRs (HEKm).[30] A high dose (3 μM) of baclofen did not affect the intracellular cAMP level in HEKm cells (Figure 5 C). This dose was considered to activate ~70% of GBRs based on the previously reported dose–response relation (EC_{50}, ~1 μM).[31] These results suggested that GBR indeed mediated the effect of baclofen on the TR-FRET signal in HEKmg12 cells. Furthermore, we confirmed that a high dose (10 μM) of DHPG did not directly affect the basal intracellular cAMP level and FK action (Figure 5 D). This dose was considered to activate ~50% of mGluR1 based on the previously reported dose-response relation (EC_{50}, ~10 μM).[19, 32]

Finally, we assessed whether and how mGluR1-mediated GBR signaling attenuation may occur in response to the endogenous GBR and mGluR1 agonists (i.e., GABA and glutamate, respectively). We measured the attenuation extent of 300 nM GABA-induced cAMP reduction in HEKmg12 cells treated with 30 nM FK. Remarkable attenuations were observed at glutamate doses of 10–300 μM but not at lower doses (Figure 5 E, $p < 0.01$, one-way ANOVA). These results suggest that activation of mGluR1 attenuates intracellular GBR signaling *in situ*.

Here, we demonstrated the interaction of mGluR1 and GBR on the cell surface (Figures 1 and 2). Several studies have shown that GPCR heterodimerization alters or fine-tunes the ligand binding, signaling, and translocation of GPCR protomers. GPCR complex formation and functional interaction play crucial roles in the regulation of neurotransmission.[33] Previously, we showed complex formation and functional interaction between mGluR1 and the adenosine A1 receptor,

which is another G_i/G_o-coupled receptor expressed in cerebellar Purkinje cells.[25, 30, 34] To further elucidate the functional interaction of GBR and mGluR1, we performed Ca^{2+} imaging in HEKmg12 cells. This analysis showed that GBR activation increased mGluR1-mediated Ca^{2+} signaling in the HEKmg12 cells (Figure 3) as described previously in cerebellar Purkinje cells.[14, 19] Pharmacological manipulation of GBR signaling showed that GBR-mediated mGluR1 signaling augmentation is independent of G_i/G_o protein, which is coupled to GBR (Figure 4 A–F). Furthermore, it appears that functional GBR containing both GBR1 and GBR2 is required to initiate mGluR1 signaling augmentation (Figure 4 G–J), although both GBR1 and GBR2 alone are able to form complexes with mGluR1 (Figure 1 G). It is possible that conformational changes in whole functional GBRs induced by GABA binding are necessary to functionally modulate mGluR1.

We also showed a clear augmentation of mGluR1 signaling occurred in response to ~60 nM GABA (Figure 3 G, H). The cerebrospinal-fluid GABA level is altered by psychotropic medication, environmental stresses, and neural activity and may affect human behavior.[35] In healthy mammalian brains, the cerebrospinal fluid contains a few tens of nM of GABA.[36] This concentration of GABA is sufficiently high to considerably activate GBR (GBR's affinity for GABA, ~1 μM[37]). In the cerebellum, vigorous excitation of parallel fibers may further increase the ambient GABA concentration by facilitating GABA release and spilt over from the parallel fiber-innervated GABAergic interneurons,[27] and ambient GABA was shown to facilitate mGluR1-mediated cerebellar LTD.[14] Therefore, GBR-mediated mGluR1 signaling augmentation may contribute to regulation of cerebellar LTD induction.

We examined whether and how mGluR1 may modulate GBR signaling by using GBR-mediated suppression of cAMP production by GBR as an index. Our homogeneous intracellular cAMP assay showed that DHPG suppressed GBR-mediated inhibition of cAMP production in a DHPG concentration-dependent manner. Our precise evaluation revealed that mGluR1 activation reduced the efficacy and potency of GBR in HEKmg12 cells (Figure 5 A, B). Treatment of 10 μM DHPG increased the EC_{50} (with DMSO, 0.078 μM; with DHPG, 0.522 μM) and

the maximal intensity (with DMSO, 0.1695 ± 0.0024; with DHPG, 0.1458 ± 0.0024) of baclofen-induced TR-FRET signal change. This result suggests that mGluR1 might serve as a competitive and noncompetitive inhibitor of GBR, inhibiting both GABA-GBR binding and GBR-G_i/G_o protein coupling. However, mGluR1 did not obviously change basal $[cAMP]_i$ or FK-induced cAMP production (Figure 5 D). We showed that glutamate (≥ 10 μM) reduced GBR signaling activated by GABA (Figure 5 E). A previous measurement of extracellular glutamate in the cerebellum indicated that several μM of glutamate may be spilt over from the parallel fibers.[38] This concentration of glutamate is sufficient to trigger mGluR1-mediated suppression of GBR signaling as shown in this study. The GBR-mediated cAMP reduction may inhibit the protein kinase A (PKA) and cAMP response element-binding protein (CREB) pathway. CREB is a transcription factor with well-documented roles in synaptic plasticity and memory formation.[39] The early phase of cerebellar LTD depends on functional modification of pre-existing proteins including receptor phosphorylation and translocation, whereas the late phase requires transcription and *de novo* protein synthesis under the control of CREB, at least in cultured Purkinje cells.[40] Because GBR-G_i/G_o signaling is expected to attenuate the PKA-CREB pathway, mGluR1-mediated inhibition of GBR might have a supportive role in the induction of mGluR1-dependent cerebellar LTD. Furthermore, in cerebellar Purkinje cells, GBR activation leads to the opening of G protein-coupled inwardly rectifying potassium (GIRK) channels and inhibits the intrinsic excitability of cerebellar Purkinje cells.[41] A decrease in the excitability may hamper cerebellar LTD induction by inhibiting Ca^{2+} opening. Glutamate-induced, mGluR1-mediated GBR modulation may restore the excitability inhibited via GIRK channels. Taken together, the functional interaction of these GPCRs may enhance cerebellar LTD and its associated motor learning by promoting mGluR1 signaling, membrane excitability, and/or gene expression in Purkinje cells.

Possible Molecular Basis for an Interaction between mGluR1 and GBR

Our results indicate that only some GPCRs may interact with each other on the plasma

membrane. This finding can be explained by that of previous studies, which showed that localization of the mGluR1 and GBR membranes is regulated by individual trafficking systems and scaffold proteins.[42, 43] When all GPCRs form a complex, they are identically regulated in function and trafficking. This diverse spectrum of GPCR interaction may be valuable to extend the range of signal transduction.

mGluR1 and GBR belong to class C GPCRs including taste and calcium-sensing receptors. The GPCRs of this class possess a large extracellular ligand-binding domain and form obligatory dimers providing a unique mode of activation compared to the GPCRs of other classes.[44] mGluR1 subunits form a homodimer via their N-termini,[45] while GBR1 and GBR2 form a heterodimer via their C-termini.[8] As these termini are utilized for forming functional mGluR1 and GBR, the transmembrane regions might be responsible for complex formation between functional mGluR1 and GBR as shown for heterodimerization between other GPCRs.[9] Previous structural analyses have shown that conformational change in the transmembrane region is important for mGluR1 activation[46] or interaction between GBR and G-protein.[47] Our findings indicate that the GPCRs further form higher-order oligomers on the cell surface. Recent studies using live imaging techniques have revealed that the structural changes and rearrangements of dimerized GPCR subunits are key events for enabling signaling by functional GPCRs.[48, 49] Such physical dynamics might underlie the functional interaction between mGluR1 and GBR. Our findings showed that the distinct functional GPCRs, each of which plays a distinct role by itself, assemble into higher-order complexes and obtain the ability to exert inter-GPCR modulation. This mechanism may help diversification of intercellular communication including synaptic transmission between neurons.

Methods

Cell Lines

We established stable cell lines expressing both mGluR1 and GBR in a Tet-inducible manner as described.[30] Briefly, we first used the Flp-In T-REx system (Invitrogen, CA, USA) to stably integrate mGluR1 cDNA into a Flp recombination site in the genome. A stable HEK293 cell line was thus obtained (HEKm), in which expression of mGluR1 could be induced with Dox. We then used the Jump-In system to integrate GBR1 and GBR2 cDNAs into several genomic hotspots using PhiC31 integrase. GBR1 and GBR2 cDNAs are inserted into pcDNA3/TO-GW-PhiC31. Their expression could be induced by Dox treatment. As resulting clones express GBR1 and GBR2 at variable levels, it was possible to select a clone with expression of mGluR1, GBR1, and GBR2.

After selection with G418, blasticidin and hygromycin, we obtained three cell lines, HEKmg1 (coexpressed mGluR1 and GBR1), HEKmg2 (mGluR1 and GBR2), and HEKmg12 (mGluR1, GBR1, and GBR2). These cell lines were treated with 2 μM Dox to induce expression and analyzed 16–24 h thereafter, at which point receptors have not yet been overexpressed.

Coimmunoprecipitation (Co-IP)

mGluR1, GBR1, and GBR2 were immunoprecipitated as described elsewhere.[34] Briefly, HEK293 cells were lysed at 4 °C for 20 min in RIPA buffer consisting of 1% Nonidet P-40, 0.5% sodium deoxycholate, 0.1% SDS, 25 mM Tris-HCl pH 7.5, 137 mM NaCl, 3 mM KCl, and protease inhibitor cocktail (Complete, Roche Diagnostics, Mannheim, Germany). Cell lysates were incubated at 4 °C for at least 12 h with antibodies bound to protein A magnetic beads (Invitrogen). The supernatants (unbound) were incubated at room temperature for 1 h with lithium dodecyl sulfate (LDS) sample buffer with dithiothreitol (DTT). Immunoprecipitates (bound) were washed four times with cold RIPA buffer, and bound proteins were eluted at room temperature for 1 h with 2× LDS sample buffer with DTT. The bound and unbound proteins were electrophoresed and immunoblotted as described elsewhere.[50] For co-IP experiments using neural tissue, we isolated synaptosomal

fractions from rat cerebellum as described elsewhere.[51] Briefly, whole female rat cerebellum was homogenized with ice-cold buffer containing 0.32 M sucrose, 10 mM Tris-HCl (pH 7.5) and protease inhibitor cocktail. A homogenized sample was centrifuged at 1000× g at 4°C for 10 min, and the supernatant was centrifuged at 17,000× g at 4°C for 30 min. The precipitate was solubilized by RIPA buffer containing the protease inhibitor mixture and centrifuged at 20,000 × g at 4°C for 60 min. The supernatant was used for co-IP as performed in HEK293 cell lysates.

Immunofluorescence and TIRF Imaging

HEKmg12 cells in glass-bottom dishes were fixed at 4 °C for 20 min with 0.1 M sodium phosphate buffer containing 4 % paraformaldehyde (PFA). Samples were then rinsed with phosphate-buffered saline (PBS) and then incubated at room temperature for 30 min in PBS supplemented with 0.1 % Triton X-100 and 5 % horse serum.[52] Cells were then probed at 4 °C overnight with 1 μg/mL primary antibody against mGluR1, GBR1, or GBR2 and subsequently stained at room temperature for 2.5 h with 5 μg/mL fluorescently labeled secondary antibodies. The cells were examined under an inverted microscope (IX71, Olympus, Tokyo, Japan) with an Orca-ER cooled CCD camera (Hamamatsu Photonics, Hamamatsu, Japan). For multicolor TIRF microscopy, we used a Leica AM TIRF MC custom-equipped from the manufacturer with a 100×, 1.46 numerical aperture (NA) oil-immersion objective (Leica Microsystems, Wetzlar, Germany); 405, 488, 561, and 635 nm lasers; and the EM-CCD camera system (ImagEM; Hamamatsu Photonics). The line scan of fluorescent intensity was performed as follows. We drew an arrow across the cell in a merged picture and plotted the distance from the root of the arrow (horizontal) and fluorescent intensity of each dye (vertical). Fluorescent intensities were measured by a built-in function of the Leica LAS AF microscope software platform (Leica Microsystems).

Antibody Patching

Patching experiments were performed as described elsewhere for Neuro2a cells.[50] Briefly, HEKmg12 cells were treated with Dox for 16–24 h. For patching of GBR1, living HEKmg12 cells were incubated with anti-GBR1 antibody (extracellular domain-reactive) as primary antibody, followed by fluorescently labeled (Alexa Fluor 488; AF488) secondary antibody. Each antibody treating step was performed at 11°C for 1 h. After GBR1 patching, cells were fixed by 4% PFA and treated with PBS containing 0.1 % of Triton X-100 and 5 % horse serum. Blocked and permeabilized cells were incubated with anti-GBR2, anti-mGluR1, or anti-Na^+/K^+-ATPase (NAKA) and then AF594-labeled secondary antibody. To exclude the possibility that nonspecific interactions caused antibody patching, we used the antibody to NAKA, an endogenous plasma membrane protein, as a control, as NAKA is expected to be segregated from the GBR1 patches. Conversely, GBR1-GBR2 may indicate higher coaccumulation, as cell surface GBR1 exists as a heterodimer with GBR2. Each antibody treatment was performed for 1 h at 11°C. The cells were examined as described in TIRF imaging. To calculate Pearson's coefficient correlation, we used built-in function of the Leica LAS AF microscope software platform (Leica Microsystems). An in-focus region of images was selected with a region of interest tool to surround one whole cell. Data were collected from randomly chosen 12 cells in each group. We used R and “bee swarm” package for statistical tests and drawing bee swarm and box plot.[53, 54]

Ca^{2+} Imaging

HEK293 cells cultured on the plastic film (LF1 Sumilon, Tokyo, Japan) were incubated with 1 μM fura-2 acetyloxymethyl ester (Dojindo, Kumamoto, Japan) in the culture medium at 37 °C for 30 min. Then, the plastic film with the cells was transferred to the recording chamber that was perfused at a rate of 0.9 mL/min with a bath solution consisting of (in mM) 147 NaCl, 3 KCl, 2 $CaCl_2$, 1 $MgCl_2$, 10 HEPES, and 10 D-glucose (pH, adjusted to 7.4 with NaOH; 25 °C). Bath solutions containing conditioning and/or test drugs were applied through the separate barrels of a theta-tube located near the examined cells. The flow of these solutions was driven by gravity and controlled by electromagnetic valves. Fluorometry was performed using a Polychrome II imager (T.I.L.L. Photonics, Planegg, Germany) attached to a BX51WI upright microscope (Olympus)

equipped with a UMPlanFL N water-immersion objective lens (20 ×, NA 0.5, Olympus). Fura-2 inside the cells was excited at 340 and 380 nm, and the resultant fluorescent signals (F_{340} and F_{380}, respectively) were captured with exposure times of 30 and 15 ms, respectively. The frame rate was 2 Hz unless otherwise stated. For each captured frame, the outlines of single cells were encompassed with polygons, and average F_{340} and F_{380} were calculated over the area of the polygons. F_{340}/F_{380} designates the ratio of these values. The peak amplitude of a DHPG-evoked intracellular Ca^{2+} response was defined as a difference from the average of F_{340}/F_{380} over a 5-s period prior to the rise of the transient to the maximal F_{340}/F_{380} during the response. In some cells, DHPG alone evoked a relatively large intracellular Ca^{2+} response at the first trial. In such cases, baclofen-induced augmentation of DHPG-evoked response was not observed at the second trial. This was presumably because the signaling cascade coupled to mGluR1 was fully activated at the first trial. Therefore, in Figures 3 and 4, we adopted the data from the cells in which the first DHPG application evoked transients with peak amplitudes of 100–500 ‰ in F_{340}/F_{380} . A change in the intracellular Ca^{2+} concentration during a conditioning was defined as a difference between the averages of F_{340}/F_{380} over a 5-s preconditioning period and the last 5-s period of the conditioning.

Homogeneous cAMP Assay

Intracellular cAMP was measured using LANCE™ cAMP competitive immunoassay (PerkinElmer Inc., Boston, MA, USA), a homogeneous TR-FRET immunoassay designed to measure cAMP produced upon modulation of adenylyl cyclase activity in a microplate, following manufacturer instructions.

Briefly, HEKm or HEKmg12 cells were treated with 2 μM Dox for 16–24 h and suspended at a density of ~6×10^2 cells/μL in Hanks' balanced salt solution containing 5 mM HEPES, 0.1% bovine serum albumin, 0.5 mM IBMX, and AF 647-conjugated antibodies against cAMP. Suspensions were then supplemented with FK, baclofen, and/or DHPG at concentrations as indicated. Suspensions were then incubated for 30 min at room temperature. To enable the measurement of the GBR-mediated reduction in the intracellular cAMP, the basal intracellular cAMP was raised by a treatment with FK and IBMX. Subsequently, cells were incubated with LANCE™ detection buffer containing the europium-labeled streptavidin, the biotin-cAMP, and Triton X-100 for 60 min at room temperature. TR-FRET was measured using a FLEX station III multimode plate reader (Molecular

Devices Inc. CA. USA). Fluorescence intensity was measured at emission of 665 and 615 nm (Em665 and Em615), with excitation at 350 nm. The Em665 can be used directly for analysis of cAMP, and the Em615 is useful in identifying dispensing or quenching problems. In this report, the ratio of Em665 to Em615 (TR-FRET signal) was used to quantify the cAMP. We also used the bioluminescence-based cAMP assay system (cAMP Glo^{TM} and cAMP Glo MAX^{TM} Assay kit, Promega Corporation, Madison, WI, USA) to confirm the cAMP signaling.

Statistical Analyses

Statistical analyses were performed using Prism software (GraphPad Software), R[53, 54] or JMP Pro (ver. 13 and 14, SAS). Antibody patching analysis was analyzed using the Wilcoxon rank sum test with Bonferroni correction since the Pearson's correlation coefficient plots did not follow the normal distribution. The box plot represents the following values: band near the middle of the box, median; top of the box, upper quartile (Q_U); bottom of the box, lower quartile (Q_L); the box length, interquartile range (IQR); end of the upper whisker, maximum value between Q_U and Q_U+1.5*IQR; end of the lower whisker, minimum value between Q_L and Q_L-1.5*IQR. Statistical significance for fractional population data in Ca^{2+} imaging was tested with the qui-square likelihood ratio test with 95% confidence. LANCE cAMP analysis was analyzed using one-way ANOVA with a Dunnett's multiple comparison posthoc test for comparisons between multiple groups and two-way ANOVA with a Tukey-Kramer posthoc test to analyze two categorical explanatory variables. Quantitative summary data were expressed as means ± SD.

Safety

No unexpected or unusually high safety hazards were encountered.

Supporting Information

The Supporting Information is available free of charge at https://pubs.acs.org/doi/10.1021/acschemneuro.9b00599.

Table S1, list of antibodies used for experiments; Figure S1, establishment of stable HEK293 cell lines with inducible expression of mGluR1; Figure S2, measurement of intracellular cAMP; and Figure S3, bioluminescence based cAMP assay for GBR signaling in HEKmg12 cells (PDF)

AUTHOR INFORMATION

H.S., Y.K., M.A., K.I., A.I, and T.T. performed the study. H.S., Y.K., and T.T. analyzed data. H.S., Y.K., T.T., and M.K. designed the study. H.S., Y.K., T.T., and T.S. wrote the manuscript. All authors read and approved the final manuscript.

Funding

This work was supported by Grants-in-Aid for Scientific Research (KAKENHI 17K09040 and 26460707 to Y.K.; 26430012 and 18K06461 to T.T.; 16H04667 to T.S.) and grants-in-aid from the Nakatomi Foundation (to Y.K.). This study was supported in part by a grant from the Institute for Environmental & Gender-specific Medicine, Juntendo University.

Notes

The authors declare no competing financial interest.

Acknowledgements

We thank Dr. R. Shigemoto for his gift of the antibodies against GBR1. We would like to thank the Laboratory of Proteomics and Biomolecular Science, Morphology and Image Analytics, and Biomedical Research Resources, Research Support Center, Juntendo University Graduate School of Medicine for technical assistance. We would like to thank Editage for English language editing.

REFERENCES

1. Barabási, A. L.; Gulbahce, N.; Loscalzo, J., Network medicine: a network-based approach to human disease. *Nat Rev Genet* **2011,** *12* (1), 56-68.

2. Franco, R.; Casadó, V.; Ciruela, F.; Saura, C.; Mallol, J.; Canela, E. I.; Lluis, C., Cell surface adenosine deaminase: much more than an ectoenzyme. *Prog Neurobiol* **1997,** *52* (4), 283-94.

3. Boyden, E. S.; Katoh, A.; Raymond, J. L., Cerebellum-dependent learning: the role of multiple plasticity mechanisms. *Annu Rev Neurosci* **2004,** *27*, 581-609.

4. Pierce, K. L.; Premont, R. T.; Lefkowitz, R. J., Seven-transmembrane receptors. *Nat Rev Mol Cell Biol* **2002,** *3* (9), 639-50.

5. Jones, K. A.; Borowsky, B.; Tamm, J. A.; Craig, D. A.; Durkin, M. M.; Dai, M.; Yao, W. J.; Johnson, M.; Gunwaldsen, C.; Huang, L. Y.; Tang, C.; Shen, Q.; Salon, J. A.; Morse, K.; Laz, T.; Smith, K. E.; Nagarathnam, D.; Noble, S. A.; Branchek, T. A.; Gerald, C., $GABA_B$ receptors function as a heteromeric assembly of the subunits $GABA_BR1$ and $GABA_BR2$. *Nature* **1998,** *396* (6712), 674-9.

6. Kaupmann, K.; Malitschek, B.; Schuler, V.; Heid, J.; Froestl, W.; Beck, P.; Mosbacher, J.; Bischoff, S.; Kulik, A.; Shigemoto, R.; Karschin, A.; Bettler, B., $GABA_B$-receptor subtypes assemble into functional heteromeric complexes. *Nature* **1998,** *396* (6712), 683-7.

7. Kuner, R.; Köhr, G.; Grünewald, S.; Eisenhardt, G.; Bach, A.; Kornau, H. C., Role of heteromer formation in $GABA_B$ receptor function. *Science* **1999,** *283* (5398), 74-7.

8. Marshall, F. H.; Jones, K. A.; Kaupmann, K.; Bettler, B., GABAB receptors - the first 7TM heterodimers. *Trends Pharmacol Sci* **1999,** *20* (10), 396-9.

9. Ferré, S.; Casadó, V.; Devi, L. A.; Filizola, M.; Jockers, R.; Lohse, M. J.; Milligan, G.; Pin, J. P.; Guitart, X., G protein-coupled receptor oligomerization revisited: functional and pharmacological perspectives. *Pharmacol Rev* **2014,** *66* (2), 413-34.

10. Thach, W. T.; Goodkin, H. P.; Keating, J. G., THE CEREBELLUM AND THE ADAPTIVE COORDINATION OF MOVEMENT. *Annu. Rev. Neurosci.* **1992,** *15*, 403-442.

11. Ito, M., The molecular organization of cerebellar long-term depression. *Nat Rev Neurosci* **2002,** *3* (11), 896-902.

12. Kulik, A.; Nakadate, K.; Nyíri, G.; Notomi, T.; Malitschek, B.; Bettler, B.; Shigemoto, R., Distinct localization of $GABA_B$ receptors relative to synaptic sites in the rat cerebellum and ventrobasal thalamus. *Eur J Neurosci* **2002,** *15* (2), 291-307.

13. Ige, A. O.; Bolam, J. P.; Billinton, A.; White, J. H.; Marshall, F. H.; Emson, P. C., Cellular and sub-cellular localisation of $GABA_{B1}$ and $GABA_{B2}$ receptor proteins in the rat cerebellum. *Mol Brain Res* **2000,** *83* (1-2), 72-80.

14. Kamikubo, Y.; Tabata, T.; Kakizawa, S.; Kawakami, D.; Watanabe, M.; Ogura, A.; Iino, M.; Kano, M., Postsynaptic $GABA_B$ receptor signalling enhances LTD in mouse cerebellar Purkinje cells. *J Physiol* **2007,** *585* (2), 549-563.

15. Rives, M. L.; Vol, C.; Fukazawa, Y.; Tinel, N.; Trinquet, E.; Ayoub, M. A.; Shigemoto, R.; Pin, J. P.; Prézeau, L., Crosstalk between $GABA_B$ and mGlu1a receptors reveals new insight into GPCR signal integration. *EMBO J* **2009,** *28* (15), 2195-208.

16. Huang, E. P., Synaptic transmission: spillover at central synapses. *Curr Biol* **1998,** *8* (17), R613-5.

17. Scanziani, M., GABA spillover activates postsynaptic $GABA_B$ receptors to control rhythmic hippocampal activity. *Neuron* **2000,** *25* (3), 673-81.

18. Walker, J. E., Glutamate, GABA, and CNS disease: a review. *Neurochem Res* **1983,** *8* (4), 521-50.

19. Tabata, T.; Araishi, K.; Hashimoto, K.; Hashimotodani, Y.; van der Putten, H.; Bettler, B.; Kano, M., Ca^{2+} activity at $GABA_B$ receptors constitutively promotes metabotropic glutamate signaling in the absence of GABA. *Proc Natl Acad Sci U S A* **2004,** *101* (48), 16952-7.

20. Hirono, M.; Yoshioka, T.; Konishi, S., $GABA_B$ receptor activation enhances mGluR-mediated responses at cerebellar excitatory synapses. *Nat Neurosci* **2001,** *4* (12), 1207-16.

21. Pandya, N. J.; Klaassen, R. V.; van der Schors, R. C.; Slotman, J. A.; Houtsmuller, A.; Smit, A. B.; Li, K. W., Group 1 metabotropic glutamate receptors 1 and 5 form a protein complex in mouse hippocampus and cortex. *Proteomics* **2016,** *16* (20), 2698-2705.

22. Schwenk, J.; Pérez-Garci, E.; Schneider, A.; Kollewe, A.; Gauthier-Kemper, A.; Fritzius, T.; Raveh, A.; Dinamarca, M. C.; Hanuschkin, A.; Bildl, W.; Klingauf, J.; Gassmann, M.; Schulte, U.; Bettler, B.; Fakler, B., Modular composition and dynamics of native $GABA_B$ receptors identified by high-resolution proteomics. *Nat Neurosci* **2016,** *19* (2), 233-42.

23. Axelrod, D., Chapter 7: Total internal reflection fluorescence microscopy. *Methods Cell Biol* **2008,** *89*, 169-221.

24. Luján, R.; Roberts, J. D.; Shigemoto, R.; Ohishi, H.; Somogyi, P., Differential plasma membrane distribution of metabotropic glutamate receptors mGluR1 alpha, mGluR2 and mGluR5, relative to neurotransmitter release sites. *J Chem Neuroanat* **1997,** *13* (4), 219-41.

25. Nonobe, Y.; Yokoyama, T.; Kamikubo, Y.; Yoshida, S.; Hisajima, N.; Shinohara, H.; Shiraishi, Y.; Sakurai, T.; Tabata, T., Application of surface plasmon resonance imaging to monitoring G protein-coupled receptor signaling and its modulation in a heterologous expression system. *BMC Biotechnol.* **2016,** *16*, 36

26. Xu, W.; Wong, T. P.; Chery, N.; Gaertner, T.; Wang, Y. T.; Baudry, M., Calpain-mediated mGluR1alpha truncation: a key step in excitotoxicity. *Neuron* **2007,** *53* (3), 399-412.

27. Dittman, J. S.; Regehr, W. G., Mechanism and kinetics of heterosynaptic depression at a cerebellar synapse. *J Neurosci* **1997,** *17* (23), 9048-59.

28. Bettler, B.; Kaupmann, K.; Mosbacher, J.; Gassmann, M., Molecular structure and physiological functions of $GABA_B$ receptors. *Physiol Rev* **2004,** *84* (3), 835-67.

29. New, D. C.; An, H.; Ip, N. Y.; Wong, Y. H., $GABA_B$ heterodimeric receptors promote Ca^{2+} influx via store-operated channels in rat cortical neurons and transfected Chinese hamster ovary cells. *Neuroscience* **2006,** *137* (4), 1347-58.

30. Kamikubo, Y.; Tabata, T.; Sakairi, H.; Hashimoto, Y.; Sakurai, T., Complex formation and functional interaction between adenosine A1 receptor and type-1 metabotropic glutamate receptor. *J. Pharmacol. Sci.* **2015,** *128* (3), 125-130.

31. Howe, J. R.; Sutor, B.; Zieglgänsberger, W., Baclofen reduces post-synaptic potentials of rat cortical neurones by an action other than its hyperpolarizing action. *J Physiol* **1987,** *384*, 539-69.

32. Wiśniewski, K.; Car, H., (S)-3,5-DHPG: a review. *CNS Drug Rev* **2002,** *8* (1), 101-16.

33. Satake, H.; Matsubara, S.; Aoyama, M.; Kawada, T.; Sakai, T., GPCR Heterodimerization in the Reproductive System: Functional Regulation and Implication for Biodiversity. *Front Endocrinol (Lausanne)* **2013,** *4*, 100.

34. Kamikubo, Y.; Shimomura, T.; Fujita, Y.; Tabata, T.; Kashiyama, T.; Sakurai, T.; Fukurotani, K.; Kano, M., Functional cooperation of metabotropic adenosine and glutamate receptors regulates postsynaptic plasticity in the cerebellum. *J Neurosci* **2013,** *33* (47), 18661-71.

35. Lee, R.; Petty, F.; Coccaro, E. F., Cerebrospinal fluid GABA concentration: relationship with impulsivity and history of suicidal behavior, but not aggression, in human subjects. *J Psychiatr Res* **2009,** *43* (4), 353-9.

36. Böhlen, P.; Huot, S.; Palfreyman, M. G., The relationship between GABA concentrations in brain and cerebrospinal fluid. *Brain Res* **1979,** *167* (2), 297-305.

37. Sodickson, D. L.; Bean, B. P., $GABA_B$ receptor-activated inwardly rectifying potassium current in dissociated hippocampal CA3 neurons. *J Neurosci* **1996,** *16* (20), 6374-85.

38. Okubo, Y.; Sekiya, H.; Namiki, S.; Sakamoto, H.; Iinuma, S.; Yamasaki, M.; Watanabe, M.; Hirose, K.; Iino, M., Imaging extrasynaptic glutamate dynamics in the brain. *Proc Natl Acad Sci U S A* **2010,** *107* (14), 6526-31.

39. Silva, A. J.; Kogan, J. H.; Frankland, P. W.; Kida, S., CREB and memory. *Annu Rev Neurosci* **1998,** *21*, 127-48.

40. Ahn, S.; Ginty, D. D.; Linden, D. J., A late phase of cerebellar long-term depression requires activation of CaMKIV and CREB. *Neuron* **1999,** *23* (3), 559-68.

41. Tabata, T.; Haruki, S.; Nakayama, H.; Kano, M., GABAergic activation of an inwardly rectifying K^+ current in mouse cerebellar Purkinje cells. *J Physiol* **2005,** *563* (2), 443-57.

42. Terunuma, M., Diversity of structure and function of GABA. *Proc Jpn Acad Ser B Phys Biol Sci* **2018,** *94* (10), 390-411.

43. Magalhaes, A. C.; Dunn, H.; Ferguson, S. S., Regulation of GPCR activity, trafficking and localization by GPCR-interacting proteins. *Br J Pharmacol* **2012,** *165* (6), 1717-1736.

44. Bräuner-Osborne, H.; Wellendorph, P.; Jensen, A. A., Structure, pharmacology and therapeutic prospects of family C G-protein coupled receptors. *Curr Drug Targets* **2007,** *8* (1), 169-84.

45. Okamoto, T.; Sekiyama, N.; Otsu, M.; Shimada, Y.; Sato, A.; Nakanishi, S.; Jingami, H., Expression and purification of the extracellular ligand binding region of metabotropic glutamate receptor subtype 1. *J. Biol. Chem.* **1998,** *273* (21), 13089-13096.

46. Wu, H. X.; Wang, C.; Gregory, K. J.; Han, G. W.; Cho, H. P.; Xia, Y.; Niswender, C. M.; Katritch, V.; Meiler, J.; Cherezov, V.; Conn, P. J.; Stevens, R. C., Structure of a Class C GPCR Metabotropic Glutamate Receptor 1 Bound to an Allosteric Modulator. *Science* **2014,** *344* (6179), 58-64.

47. Geng, Y.; Bush, M.; Mosyak, L.; Wang, F.; Fan, Q. R., Structural mechanism of ligand activation in human $GABA_B$ receptor. *Nature* **2013,** *504* (7479), 254-9.

48. Grushevskyi, E. O.; Kukaj, T.; Schmauder, R.; Bock, A.; Zabel, U.; Schwabe, T.; Benndorf, K.; Lohse, M. J., Stepwise activation of a class C GPCR begins with millisecond dimer rearrangement. *Proc Natl Acad Sci U S A* **2019,** *116* (20), 10150-10155.

49. Xue, L.; Sun, Q.; Zhao, H.; Rovira, X.; Gai, S.; He, Q.; Pin, J. P.; Liu, J.; Rondard, P., Rearrangement of the

transmembrane domain interfaces associated with the activation of a GPCR hetero-oligomer. *Nat Commun* **2019,** *10* (1), 2765.

50. Sakurai, T.; Kaneko, K.; Okuno, M.; Wada, K.; Kashiyama, T.; Shimizu, H.; Akagi, T.; Hashikawa, T.; Nukina, N., Membrane microdomain switching: a regulatory mechanism of amyloid precursor protein processing. *J Cell Biol* **2008,** *183* (2), 339-52.

51. Kamikubo, Y.; Sakurai, T., Co-immunoprecipitation Analysis of GPCR Complexes in the Central Nervous System. *Neuromethods* **2019**, 144, 49-64.

52. Kamikubo, Y.; Egashira, Y.; Tanaka, T.; Shinoda, Y.; Tominaga-Yoshino, K.; Ogura, A., Long-lasting synaptic loss after repeated induction of LTD: independence to the means of LTD induction. *Eur J Neurosci* **2006,** *24* (6), 1606-16.

53. R Core Team *R: A language and environment for statistical computing,* R Foundation for Statistical Computing. **2018**

54. Eklund, A. *beeswarm: The Bee Swarm Plot, an Alternative to Stripchart.* **2016**

FIGURE LEGENDS

Figure 1. Complex formation of GPCRs at the rat cerebellum or at HEK293 cells.

(A) Co-IP of GBR1 and GBR2 with mGluR1 in the lysate of synaptosomal fractions derived from the rat cerebellum. Lysates of synaptosomal fractions were immunoprecipitated with anti-mGluR1 or control IgG (Ctrl IgG). The supernatants (unbound) and precipitates (bound) were electrophoresed and immunoblotted with the labeled antibodies. (B) Co-IP of mGluR1 or GBR2 with GBR1 in the lysates of synaptosomal fractions derived from the rat cerebellum. (C) Co-IP of GBR1 and GBR2 with mGluR1 in lysates of tagged GPCRs-transfected HEK293 cells. Venus-tagged mGluR1, HA-tagged GBR1, and VSVG-tagged GBR2 were transfected into HEK cells. Lysates were immunoprecipitated with anti-GFP antibody or control IgG. The supernatants and precipitates were immunoblotted with an antibody against mGluR1, HA, or VSVG. (D) To examine the expression of GPCRs, the lysates of the established HEK293 cell were electrophoresed and immunoblotted with antibodies against mGluR1, GBR1, GBR2, and beta-actin. HEK293 clones were treated with 2 μM Dox or vehicle for 16 h. Cells were lysed with RIPA buffer and analyzed. (E) Co-IP of GBR1 and GBR2 with mGluR1. Lysates from HEKmg12 (Clone #04) cells were immunoprecipitated with anti-mGluR1 or control IgG. The supernatants and precipitates were immunoblotted with the labeled antibodies. (F) Co-IP of mGluR1 with GBR1 or GBR2. Lysates from HEKmg12 cells were immunoprecipitated with anti-GBR1, GBR2, or control IgG. The supernatants and precipitates were immunoblotted with the labeled antibodies. (G) Co-IP of GBR1 and GBR2 with mGluR1. Lysates from HEKmg1 (Clone #01) or HEKmg2 (Clone #03) cells were immunoprecipitated with anti-mGluR1 or control IgG. The supernatants and precipitates were immunoblotted with the labeled antibodies. GBR1 and GBR2 alone can form complexes with mGluR1, although they differ in their affinity to mGluR1.

Figure 2. Cell surface colocalization and interaction of GBR and mGluR1.

(A) TIRF microscopic images of HEK293 cells transfected with tagged GPCRs. SNAP-tagged GBR1, HA-tagged mGluR1, and VSVG-tagged GBR2 were transiently transfected into HEK293 cells. Live HEK293 cells were stained with fluorescent-labeled SNAP-tag substrate and antibodies at 11°C for 1 h. GBR1 was labeled with SNAP surface 488 (cyan), mGluR1 was labeled with AF594 conjugated anti-HA antibody (magenta) and GBR2 was labeled with DL649 conjugated anti-VSVG antibody (yellow). (B, C) TIRF microscopic images and line scans of HEKmg12 cells. GBR1 (B) or GBR2 (C) was labeled with AF488 (green) and mGluR1 was labeled with AF594 (red). Line scans were analyzed on the dotted arrows shown in each figure. The horizontal axis of the graph shows the distance from the root of the arrow, and the vertical axis of the graph shows the fluorescent intensity of each fluorescent dye. (D–F) TIRF microscopic analysis of cell surface patches of GBR1 and colocalization of GBR2 and mGluR1. Live HEKmg12 cells were treated with the anti-GBR1 antibody, followed by the AF488 labeled secondary antibody at 11 °C to induce cell surface patches. After inducing patches, cells were fixed with 4% PFA, permeabilized, and treated with anti-GBR2 (D), anti-mGluR1 (E), or anti-Na^+/K^+-ATPase (NAKA) (F) antibody, followed by an AF594-labeled secondary antibody. (G) Quantitative measurements of colocalization between GBR1 patches and GBR2 (left), mGluR1 (center), or NAKA (right) in TIRF images. Pearson's correlation coefficient between the fluorescent intensity of AF488 and AF594 was calculated from 12 cells in each group. Data were analyzed using the Wilcoxon rank sum test with Bonferroni correction since the plots did not follow the normal distribution. $*p = 0.0055$; $**p = 0.0087$, scale bars: 2.5 μm.

Figure 3. GBR activation augmented the mGluR1-mediated response.

(A) Representative DHPG-evoked intracellular Ca^{2+} responses of single cells expressing GBR1, GBR2, and mGluR1 before and after conditioning with the control vehicle or the GBR agonist baclofen. Upper images, gray scale F_{380} images (scale bar, 20 μm), and pseudocolor F_{340}/F_{380} images of the cells. Lower traces, time plots of F_{340}/F_{380} obtained from the single cells (arrow heads) in the

upper images. The times at which the corresponding images were captured are indicated by integers. Solid and dotted parts of the trace, data sampled at rates of 2 and 0.25 Hz, respectively. Arrow, onset of a DHPG application (50 μM, 2 s). Thick bar, duration (12 s) of an application of the control vehicle or baclofen (30 nM). The presentation conventions in this figure also apply to the following figures. (B) Percent augmentation of the peak amplitude of the DHPG-evoked intracellular Ca^{2+} responses after conditioning with the control vehicle (22 cells) or baclofen (34 cells). The peak amplitude of the transients before the conditioning was taken as 100% for each cell. Dot, data obtained from each cell. Gray box, two quantiles around the median. Dotted line, level of 60%. (C) Percentages of the cells with % augmentations of ≥ 60% and < 60%. *, $p = 0.024$, chi-square likelihood ratio test. (D) Mean changes in F_{340}/F_{380} during conditioning with the labeled agents. Error bars are ± SEM. The data were derived from the same cells as shown in panels B and C. (E) Representative time plots of intracellular Ca^{2+} responses of single cells expressing GBR1, GBR2, and mGluR1 to time-lagged application of DHPG (5 μM, 22 s, thick bar) and the control vehicle or baclofen (30 nM) (12 s, thick bar). Although DHPG at the concentration used here did not evoke a Ca^{2+} response by itself, additionally applied baclofen enabled DHPG to evoke a transient. (F) Percentage of the examined cells displaying a Ca^{2+} response after an additional application of the labeled agents (black area). N = 46 cells for control and 37 cells for baclofen. *, $p = 0.026$, chi-square likelihood ratio test. (G) Representative time plots of intracellular Ca^{2+} responses of single cells expressing GBR1, GBR2, and mGluR1 to DHPG (50 μM, 2 s, arrows) without (first trial) and with (second trial) the labeled doses of GABA. (H) % augmentation of the peak amplitude of the DHPG-evoked Ca^{2+} responses is plotted against the coapplied GABA dose. The peak amplitude of the transient at the first trial was taken as 100%. N = 38, 15, 16, and 44 cells for 3, 30, 300, and 1000 nM, respectively. Sigmoid curve, Hill function (Hill coefficient = 1) fitted to the data.

Figure 4. GBR augmented the mGluR1-mediated response independently of G_i/G_o protein.

(A) Representative time plots of intracellular Ca^{2+} responses of single cells expressing GBR1, GBR2,

and mGluR1 to DHPG (50 μM, 2 s, arrows) before and after conditioning with the GBR agonist baclofen (30 nM, 12 s, thick bar) or the G_i/G_o protein activator mastoparan (1 μM, 100 s, thick bar). "PTX-pretreated", the cells treated with the G_i/G_o protein inhibitor PTX (500 ng/mL) for ≥ 24 h before the measurement. (B) % augmentation of the peak amplitude of the DHPG-evoked intracellular Ca^{2+} responses after conditioning. Left column, 34 nonpretreated cells conditioned with baclofen (data reproduced from Figure 3). Middle column, 52 PTX-pretreated cells conditioned with baclofen. Right column, 20 nonpretreated cells conditioned with mastoparan. (C) Percentages of the cells with % augmentations of ≥ 60% and < 60%. *** and NS, $p = 0.0009$ and $p = 0.79$, respectively; chi-square likelihood ratio test. (D) Mean changes in F_{340}/F_{380} of the cells during conditioning with baclofen (left and middle columns) or mastoparan. Error bars are ± SEM. The data were derived from the same cells as shown in panels B and C. (E) Luminescence cAMP assay to confirm that PTX inhibited the G_i/G_o protein in HEKmg12 cells. Column, mean cAMP concentration of the lysates of non-pretreated or PTX-pretreated cells measured after incubation (15 min) with baclofen (30 μM) and folskolin (30 nM). N = 5 vials for each condition. ***, $p = 0.0003$, unpaired t-test. (F) Luminescence cAMP assay to confirm that mastoparan activated the G_i/G_o protein in HEKmg12 cells. Column, mean cAMP concentration of the lysates of non-pretreated cells measured after incubation (100 s) with folskolin (30 nM) and either mastoparan (1 μM) or control vehicle. N = 7 vials for each condition. *, $p = 0.022$, unpaired t-test. (G) Representative time plots of intracellular Ca^{2+} responses of single cells expressing the labeled GBR subunits to DHPG (50 μM, 2 s, arrows) before and after conditioning with the GBR agonist baclofen (30 nM, 12 s, thick bars). (H) % augmentation of the peak amplitude of the DHPG (50 μM, 2 s)-evoked intracellular Ca^{2+} responses of cells expressing the labeled subunits after baclofen conditioning (30 nM, 12 s). N = 34 (data reproduced from Figure 3), 52, and 20 cells from the left to the right column. (I) Percentages of cells with % augmentations of ≥ 60% and < 60%. **, $p = 0.007$ for the GBR1-expessing cells and $p = 0.0022$ for the GBR2-expressing cells, chi-square likelihood ratio test. (J) Mean changes in F_{340}/F_{380} of cells expressing the labeled subunits during baclofen conditioning. Error bars are ± SEM. The data

were derived from the same cells as shown in panels H and I.

Figure 5. Activation of mGluR1 impedes GBR signaling in HEKmg12 cells.

(A) Treatment with baclofen inhibited the increase in $[cAMP]_i$ induced by FK (open circle, N = 4). Treatment with 10 μM DHPG suppressed the effect of baclofen (filled square, N = 4). Data were analyzed by two-way ANOVA to test for statistical significance and then Tukey-Kramer tests for multiple comparisons. (B) DHPG reverses the effect of 3 μM baclofen in a dose-dependent manner, at concentrations higher than 10 μM. One-way ANOVA was used to test for statistical significance, and differences between pairs were analyzed using Dunnett's multiple comparison test vs cells treated with 30 nM FK and 3 μM baclofen in the absence of DHPG. N = 12. (C) Baclofen does not affect $[cAMP]_i$ in HEKm, stably expressing mGluR1 without GBR. N = 4. (D) DHPG by itself does not block FK (30 nM)-induced increase in $[cAMP]_i$ (filled square, N = 4) or affect basal $[cAMP]_i$ (open circle, N = 4). (E) Administration of glutamate reverses the effect of 300 nM GABA in a dose-dependent manner at concentrations higher than 10 μM. One-way ANOVA was used to test for statistical significance, and differences between pairs were analyzed using Dunnett's multiple comparison test vs cells treated with 30 nM FK and 3 μM baclofen in the absence of DHPG. N = 4. Error bars are ± SD $*p < 0.05$; $**p < 0.01$; $***p < 0.001$.

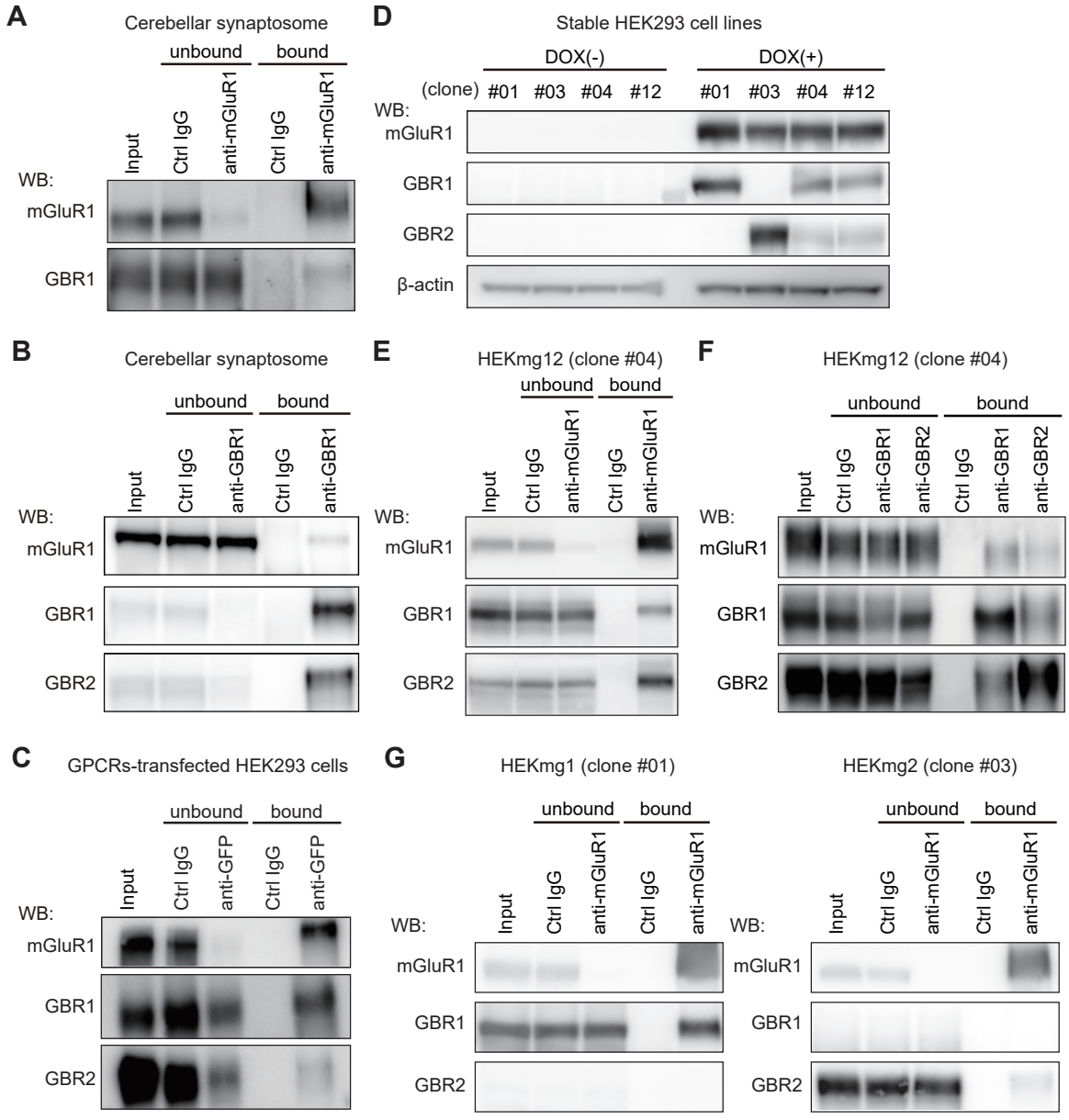

Fig.1 Sakairi et al.

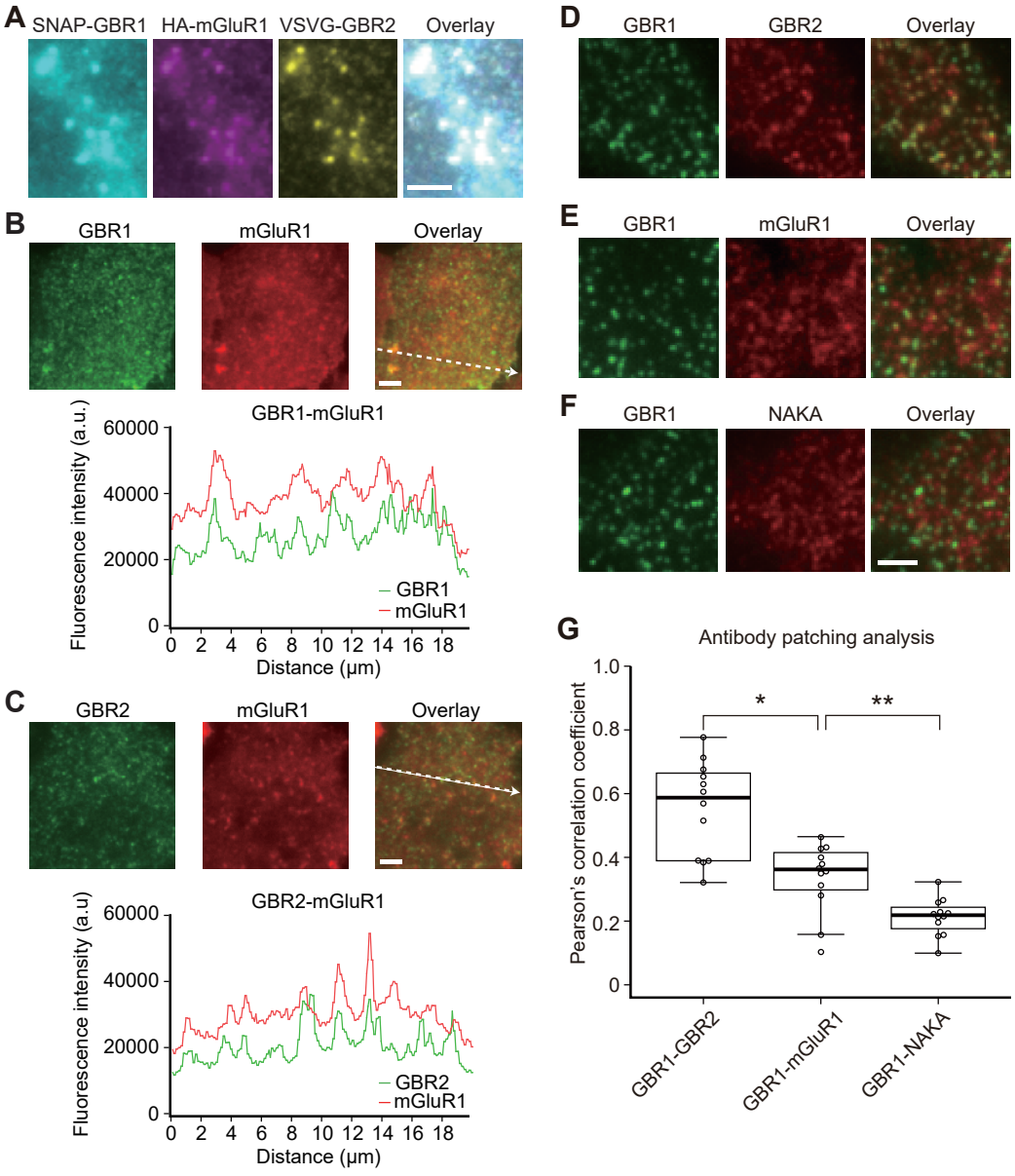

Fig.2 Sakairi et al.

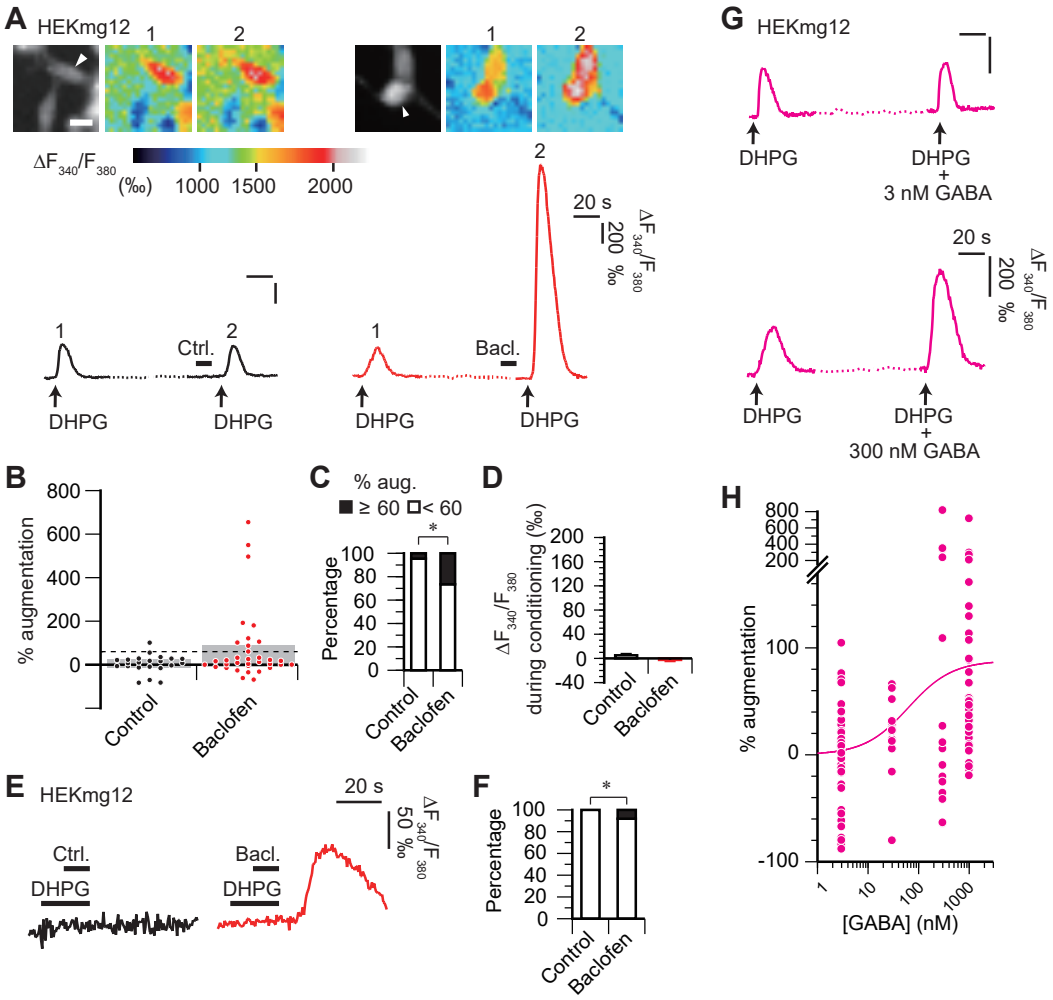

Fig. 3 Sakairi et al.,

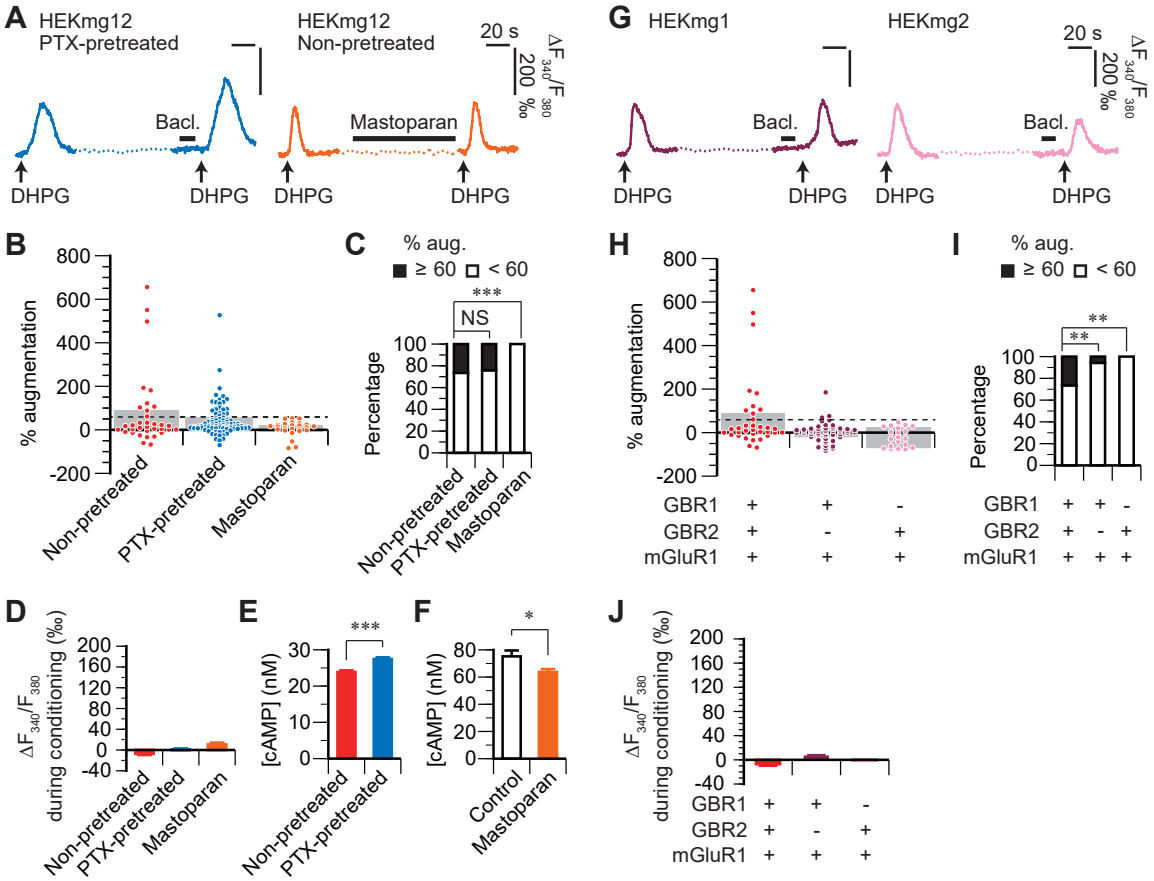

Fig. 4 Sakairi et al.,

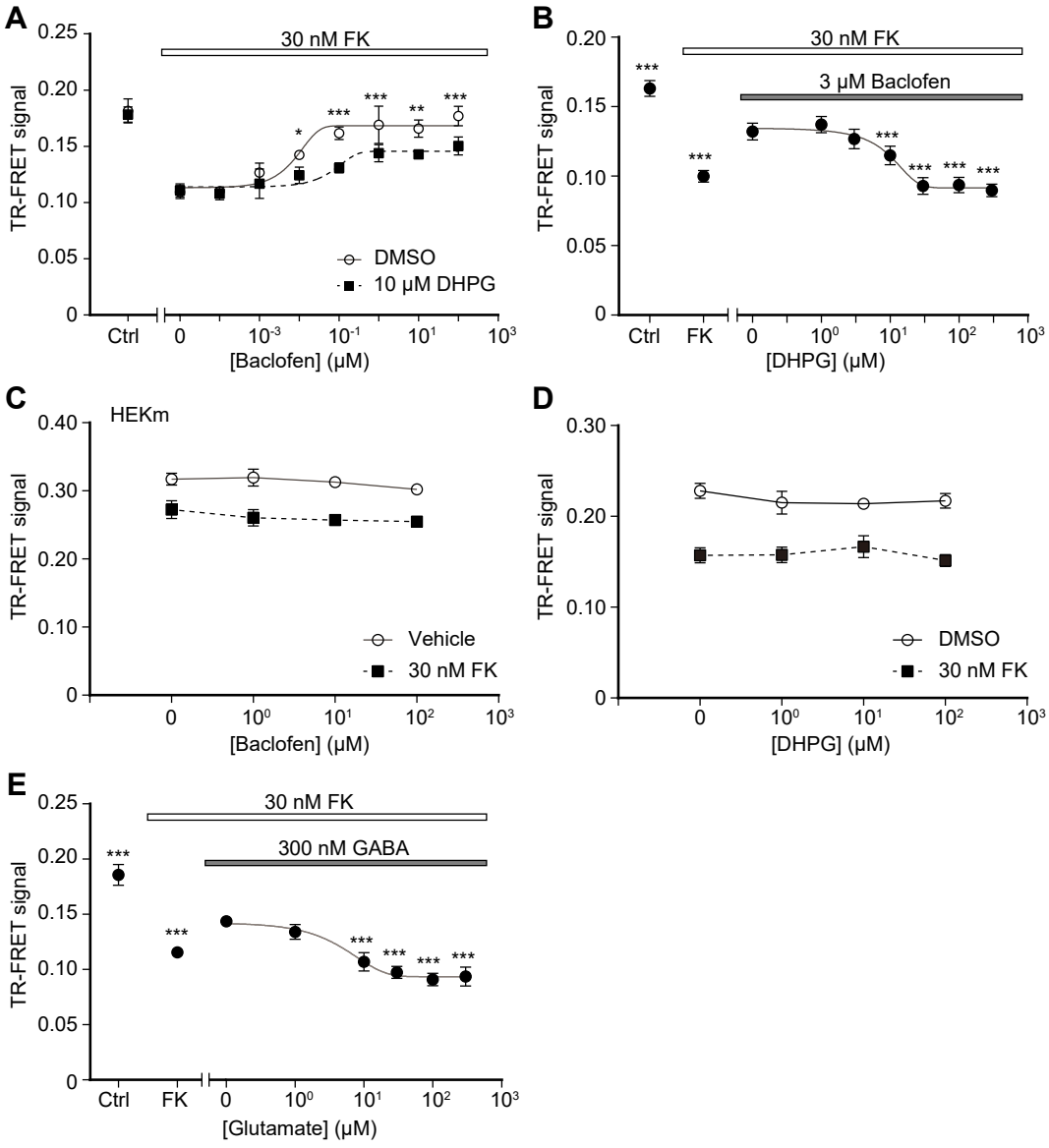

Fig.5 Sakairi et al.

Figure S1. Establishment of stable HEK293 cell lines with inducible expression of mGluR1, GBR1, and GBR2.

To examine the expression of GPCRs, cell lysates were electrophoresed and immunoblotted with antibodies against mGluR1, GBR1, GBR2, and beta-tubulin. HEKmg12 (clone #04) cells were treated with 2 μM Dox for 0 to 24 h.

Figure S2. Measurement of intracellular cAMP using the LANCE cAMP assay system.

(A-C) Densitometry of cAMP was performed using the LANCE cAMP assay system. Reactions were assembled with the indicated cAMP concentrations in a 384-well plate. The fluorescence intensity of 665 nm (A) and 615 nm (B) and ratio of 665 nm to 615 nm (C, TR-FRET signal). The TR-FRET signal showed negative correlation to the cAMP concentrations. N=4. (D) HEKmg12 cells were treated with FK or vehicle (control). Administration of FK decreased the TR-FRET signal in a dose-dependent manner. N=4. Error bars are ± SD.

Figure S3. Bioluminescence-based cAMP assay for GBR signaling in HEKmg12 cells.

(A) Densitometry of cAMP was performed using the cAMP-Glo^{TM} assay system. Reactions were assembled with the indicated concentrations of purified cAMP in a low-volume 96-well plate. Data were collected using a plate-reading luminometer. N=4. (B) Cells were treated with the indicated concentrations of FK. FK decreased cAMP-Glo luminescence in a dose-dependent manner. N=3. (C, D) DHPG by itself does not affect basal $[cAMP]_i$ (C, N=3–4), and FK (1 μM)-induced increase in $[cAMP]_i$ (D, N=6). (E) Cells were treated with the indicate concentrations of baclofen in the presence of 1 uM FK. Baclofen inhibited the increase in $[cAMP]_i$ induced by FK. N=4. One-way ANOVA was used to test for statistical significance, and differences between pairs were analyzed using Dunnett's multiple comparison test vs. cells treated with 1 μM FK in the absence of baclofen. (F) Cells were treated with the indicated concentrations of DHPG in the presence of 1 μM FK and/or 0.3 μM baclofen. DHPG reversed the effect of 0.3 μM baclofen in a dose-dependent manner, starting

at 3 μM. N=7. One-way ANOVA was used to test for statistical significance, and differences between pairs were analyzed using Dunnett's multiple comparison test vs. cells treated with 1 μM FK and 0.3 μM baclofen in the absence of DHPG. Error bars are ± SD. *$p < 0.05$; **$p < 0.01$; ***$p < 0.001$.

Table S1. List of antibodies used for experiments.

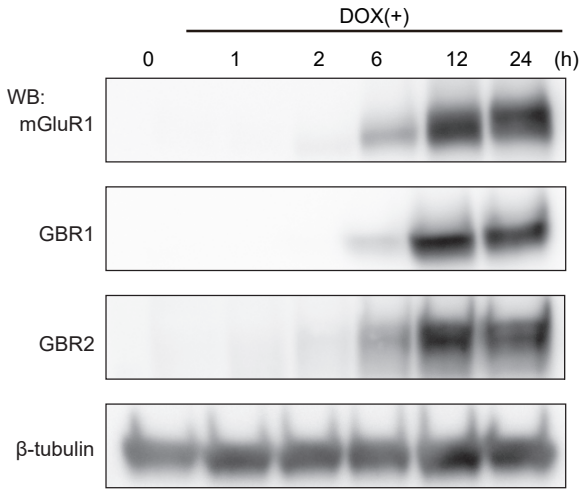

Figure S1. Establishment of stable HEK293 cell lines with inducible expression of mGluR1, GBR1, and GBR2.

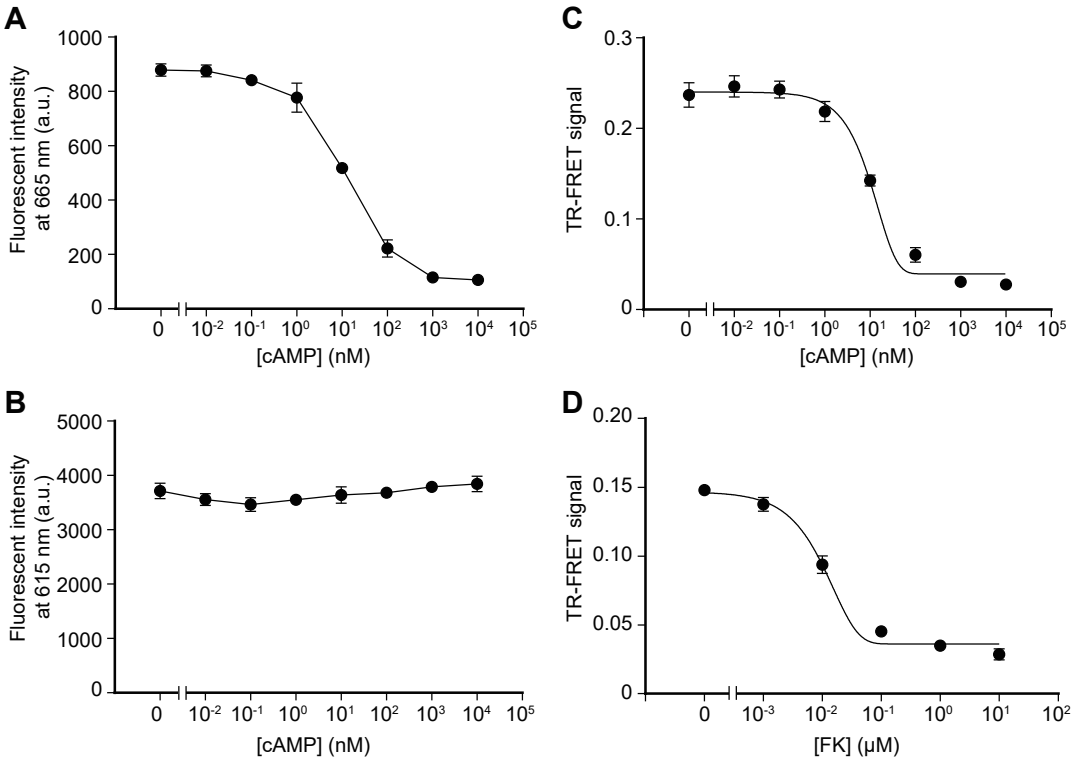

Figure S2. Measurement of intracellular cAMP using the LANCE cAMP assay system.

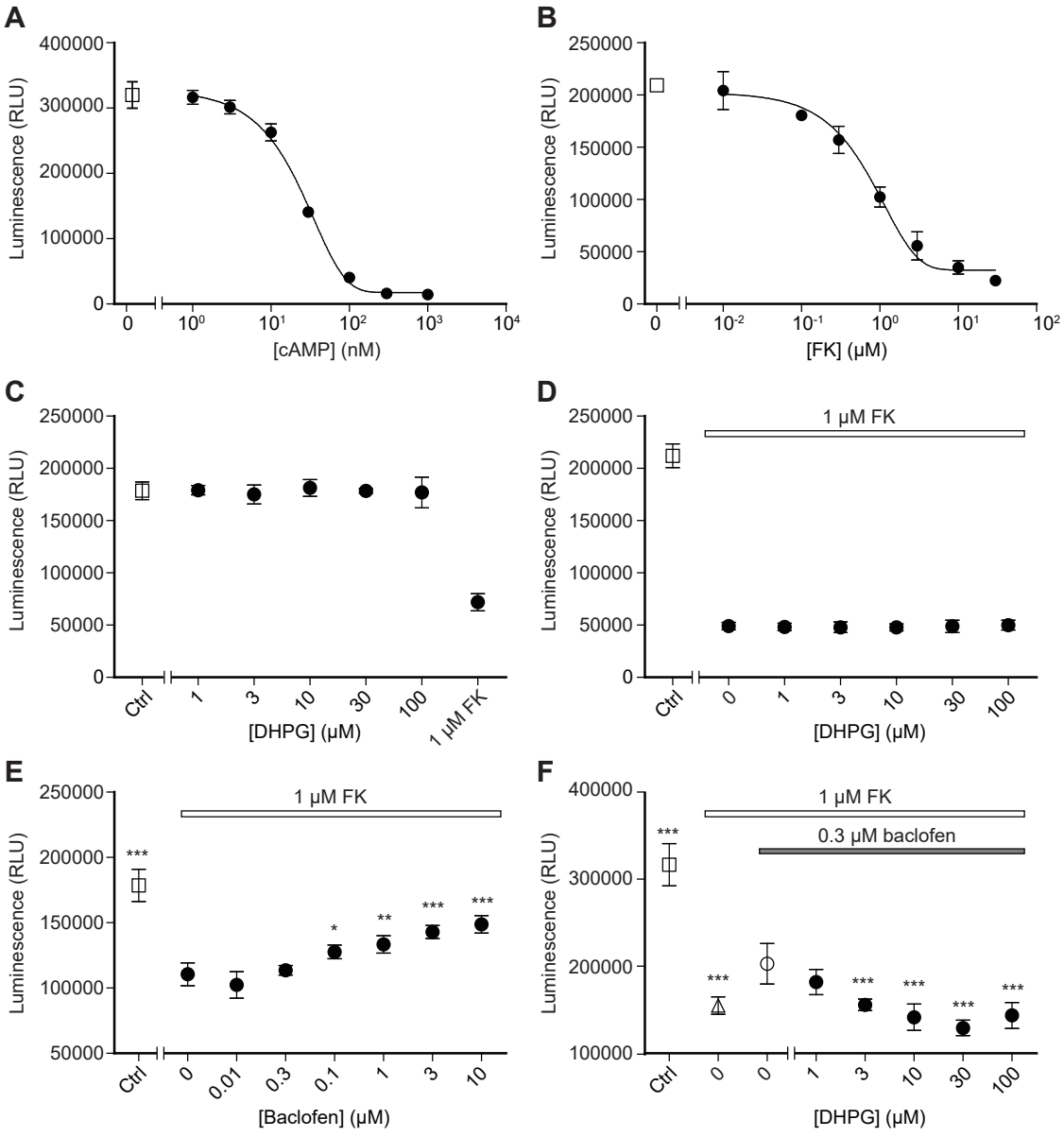

Figure S3. Bioluminescence-based cAMP assay for GBR signaling in HEKmg12 cells.

Table S1 List of antibodies used for experiments

	Antibody	Species	Supplier	Code
Immunoprecipitation	anti-GBR1	Rabbit	Invitrogen	PA5-17075
	anti-GBR2	Rabbit	Invitrogen	PA5-17035
	anti-mGluR1	Rabbit	Details are described in Kamikubo *et al*., 2013	
	anti-GFP	Mouse	Life Technologies	A11120
Immunoblot	anti-GBR1	Sheep	R&D Systems	AF7000
	anti-GBR1	Rabbit	Details are described in Kulik *et al*., 2002	
	anti-GBR2	Goat	R&D Systems	AF1188
	anti-mGluR1	Mouse	BD Biosciences	610965
	anti-mGluR1	Sheep	R&D Systems	AF4836
	anti-mGluR1	Rabbit	Details are described in Kamikubo *et al*., 2013	
	anti-HA	Rabbit	Promega	G928A
	anti-VSVG	Rabbit	Sigma-Aldrich	V4888
TIRF imaging	anti-GBR1	Rabbit	Invitrogen	PA5-17075
	anti-GBR2	Rabbit	Invitrogen	PA5-17035
	anti-mGluR1	Mouse	BD Biosciences	610965
	anti-rabbit (AF488)	Donkey	Invitrogen	A21206
	anti-mouse (AF594)	Donkey	Molecular Probes	A21203
	anti-HA (AF594)	Mouse	MBL	M180-A59
	anti-VSVG (DL649)	Rabbit	Rockland	600-443-386
Antibody patching	anti-GBR1	Sheep	R&D Systems	AF7000
	anti-GBR2	Rabbit	Invitrogen	PA5-17035
	anti-mGluR1	Rabbit	Details are described in Kamikubo *et al*., 2013	
	anti-NAKA	Rabbit	Abcam	ab76020
	anti-sheep (AF488)	Donkey	Invitrogen	A11015
	anti-rabbit (AF594)	Donkey	Life Technologies	A21207